

The frequency, intensity, and diurnal cycle of precipitation in surface and satellite observations over low- and mid-latitudes

Aiguo Dai · Xin Lin · Kuo-Lin Hsu

Received: 9 January 2007 / Accepted: 20 March 2007
© Springer-Verlag 2007

Abstract Global precipitation data sets with high spatial and temporal resolution are needed for many applications, but they were unavailable before the recent creation of several such satellite products. Here, we evaluate four different satellite data sets of hourly or 3-hourly precipitation (namely CMORPH, PERSIANN, TRMM 3B42 and a microwave-only product referred to as MI) by comparing the spatial patterns in seasonal mean precipitation amount, daily precipitation frequency and intensity, and the diurnal and semidiurnal cycles among them and with surface synoptic weather reports. We found that these high-resolution products show spatial patterns in seasonal mean precipitation amount comparable to other monthly products for the low- and mid-latitudes, and the mean daily precipitation frequency and intensity maps are similar among these pure satellite-based precipitation data sets and consistent with the frequency derived using weather reports over land. The satellite data show that spatial variations in mean precipitation amount come largely from precipitation frequency rather than intensity, and that the use of satellite infrared (IR) observations to improve sampling does not change the mean frequency, intensity and the diurnal cycle

significantly. Consistent with previous studies, the satellite data show that sub-daily variations in precipitation are dominated by the 24-h cycle, which has an afternoon–evening maximum and mean-to-peak amplitude of 30–100% of the daily mean in precipitation amount over most land areas during summer. Over most oceans, the 24-h harmonic has a peak from midnight to early morning with an amplitude of 10–30% during both winter and summer. These diurnal results are broadly consistent with those based on the weather reports, although the time of maximum in the satellite precipitation is a few hours later (especially for TRMM and PERSIANN) than that in the surface observations over most land and ocean, and it is closer to the phase of showery precipitation from the weather reports. The TRMM and PERSIANN precipitation shows a spatially coherent time of maximum around 0300–0600 local solar time (LST) for a weak (amplitude <20%) semi-diurnal (12-h) cycle over most mid- to high-latitudes, comparable to 0400–0600 LST in the surface data. The satellite data also confirm the notion that the diurnal cycle of precipitation amount comes mostly from its frequency rather than its intensity over most low and mid-latitudes, with the intensity has only about half of the strength of the diurnal cycle in the frequency and amount. The results suggest that these relatively new precipitation products can be useful for many applications.

A. Dai (✉)
National Center for Atmospheric Research,
P.O. Box 3000, Boulder, CO 80307-3000, USA
e-mail: adai@ucar.edu

X. Lin
NASA Goddard Space Flight Center,
Greenbelt, MD, USA

X. Lin
University of Maryland, Baltimore, MD, USA

K.-L. Hsu
University of California, Irvine, CA, USA

1 Introduction

Precipitation is one of the most important climate and meteorological variables. However, in situ observations of precipitation have been sparse over many land areas and

largely unavailable over the vast oceans (Dai et al. 1997; Dai 2001a; New et al. 2001). During recent decades, satellite microwave and infrared (IR) remote-sensing data have been used to derive monthly or daily precipitation over the oceans and more recently also over the land (e.g., Xie and Arkin 1997; Huffman et al. 2001; Adler et al. 2003). During the last 5–10 years, techniques have been developed to produce near real-time hourly or 3-hourly precipitation at 0.25° or better resolution for the entire Tropics and middle latitudes (approximately 60°S–60°N) (e.g., Hsu et al. 1997; Sorooshian et al. 2000; Joyce et al. 2004; Huffman et al. 2007). Because of their high temporal and spatial resolution and being near real-time, these products can be very useful in weather, climate, hydrology, and other research and applications after quantitative evaluations. Analyses by the groups who created the products (e.g., Sorooshian et al. 2000; Joyce et al. 2004; Huffman et al. 2007) revealed that the errors for individual small grid boxes can be large but it decreases rapidly with spatial and temporal averaging.

One of the applications of these high-resolution satellite precipitation products is to help study the diurnal cycle of precipitation. Although it has been well documented over the continental United States (e.g., Wallace 1975; Dai et al. 1999), where hourly rain-gauge data are available (Higgins et al. 1996), the diurnal cycle of precipitation is less quantified over many other parts of the world, especially over the open oceans because of a lack of high-resolution rainfall data [except several analyses of hourly rain-gauge data over a few small regions and some Pacific islands (see Dai 2001b for references)]. By compiling 3-hourly weather reports from stations and ships from 1975 to 1997, Dai (2001b) produced the only global result of diurnal cycle of precipitation frequency from in situ observations. Satellite observations have been analyzed to document the diurnal cycle of precipitation, mostly over the low latitudes (e.g., Janowiak et al. 1994; Chang et al. 1995; Sorooshian et al. 2002; Nesbitt and Zipser 2003; Bowman et al. 2005; Hong et al. 2005; Yang and Smith 2006). These satellite-based studies have improved our knowledge about the diurnal cycle of precipitation, especially over tropical oceans. However, there are indications that remotely-sensed precipitation (i.e., from ground-based radars and satellites) may have slightly different diurnal phase than that based on rain-gauge data (Liang et al. 2004; Dai 2006). Given that radars and satellite-borne radiometers directly measure precipitation-process-related reflectivity or radiance, not surface precipitation, it is not surprising to see differences in the diurnal phase and amplitude revealed by surface and satellite observations. As satellite data have been increasingly used to study the sub-daily variations in precipitation and atmospheric convection (Lin et al. 2000; Yang and Slingo 2001), it becomes important to compare and quantify the differences in the diurnal cycle of precipitation

shown by surface and satellite observations and among the different satellite products. Although limited surface observations have been used in some of the analyses of satellite data (e.g., Janowiak et al. 1994; Bowman et al. 2005; Pinker et al. 2006), a comprehensive comparison has been unavailable and is one of the main goals of this study.

The previous analyses of surface and satellite precipitation data have shown coherent diurnal variations in tropical and mid-latitude precipitation, with larger relative amplitudes over land areas (up to 100% of the daily mean) during warm seasons than over oceans. In general, warm-season precipitation over land areas is more frequent during the afternoon [1400–1800 local solar time (LST)], whereas the maximum rainfall is from midnight to early morning (2200–0600 LST) over the oceans and small islands (e.g., Dai 2001b; Bowman et al. 2005; Yang and Smith 2006). Many of the oceans and their adjacent continents have an out-of-phase diurnal cycle in precipitation and surface wind fields (Dai and Deser 1999; Dai 2001b). There are, however, exceptions to this general pattern. For example, summer precipitation is most frequent from middle night to early morning in the central US (Wallace 1975; Dai et al. 1999), southeast China, and a few other regions (Dai 2001b). These nocturnal maxima are often associated with a nocturnal environment with little inhibition to convective onset (Trier and Parsons 1993) and downwind propagation of convective systems in the lee of mountains (Carbone et al. 2002; Okumura et al. 2003; Wang et al. 2004; Fujinami et al. 2005), whereas afternoon convection is suppressed by large-scale subsidence over the central US (Dai et al. 1999). During cold seasons, precipitation has a much weaker diurnal cycle than in summer, with a morning maximum in winter over most land areas that is at least partially enhanced by the morning maximum in lower tropospheric relative humidity (Dai et al. 1999; Dai 2001b), as higher relative humidity increases formation of condensates. Hourly rain-gauge data from the US (Dai et al. 1999) and Japan and Malaysia (Oki and Musiak 1994) show that precipitation diurnal cycle comes mostly from precipitation frequency rather than intensity, which has a much weaker diurnal cycle than frequency. Although a single large peak is a dominant feature in most station rain-gauge records, there is a secondary peak or a weak semidiurnal (12 h) cycle of rainfall at many tropical (peak around 0300 LST) and mid-latitude (peak around 0600 LST) stations (Hamilton 1981; Oki and Musiak 1994).

Here we make use of our knowledge about the diurnal cycle of precipitation to evaluate the existing high-resolution precipitation products derived from multi-satellite observations. We compare the diurnal phase and amplitude revealed by various satellite products and also with those from surface observations. Some of the satellite products use IR observations from geostationary satellites to im-

prove temporal sampling, which is only 1–2 times per day for microwave sensors on-board a single polar orbiting satellite. Since the IR sensors measure radiance from cloud tops rather than hydrometeors within clouds (i.e., ice particles, and cloud and rain droplets that are more directly related to precipitation), whose radiance is measured by microwave sensors, it is unclear whether the inclusion of the IR data has any effects on the representation of the diurnal cycle and other precipitation characteristics (e.g., frequency and intensity) by the derived products. We investigate this effect by comparing products with and without IR observations. After the comparison and evaluation, we also apply the satellite data to further quantify the diurnal variations in tropical and mid-latitude precipitation, especially over regions (e.g., oceans) where surface observations are sparse. For example, the satellite data can help us verify whether it is true over most of the globe that precipitation diurnal cycle comes mostly from its variations in frequency rather than intensity, as seen over the U.S. Our analyses provide further evaluation of the high-resolution data sets and new results on the diurnal cycle of precipitation over the low- and mid-latitudes. This paper focuses on the global and large-scale features; detailed regional analyses will be done in a separate study.

2 Data and analysis method

The satellite and surface data sets used for this study are summarized in Table 1 with references and web links. They include four merged or blended precipitation data sets derived from multi-satellite observations using motion vectors in infrared images (CMORPH), neural networks (PERSIANN), IR estimates calibrated by microwave estimates from TRMM and other satellites (TRMM 3B42), and a microwave-only products created by simply merging estimates from five satellites (MI). Furthermore, the CMORPH data set also contains a microwave-only version (CMORPHmi) that is included in this study. The CMORPH data set was used by Xie et al. (2005) to study the diurnal cycle in the North American Monsoon. Although MI and CMORPHmi are both microwave-only products, they differ in the satellite sensors included (Table 1) and algorithms used to estimate rainfall: MI used the Goddard Profiling (GPROF) version 6 algorithm for all the satellites, while CMORPHmi used different algorithms for different satellite sensors (Joyce et al. 2004). For surface in situ observations, we used the long-term (1976–1997) mean 3-hourly data of precipitation occurrence frequency derived from weather reports by Dai (2001b). For the U.S., there are hourly rain-gauge data available. We will present detailed comparisons with this and other regional data sets in a separate study.

These satellite products cover only the last several years, with better sampling by microwave sensors since late 2001. Tests with the U.S. rain-gauge data showed that a stable diurnal cycle may be obtained with just several years of data. In order to derive a robust mean diurnal cycle with sufficient sampling and in the meantime have comparable data periods, we averaged the data (stratified by each observation hour and each season) over 2003–2005 for CMORPH, 2002–2005 for PERSIANN (similar results for 2003–2005), 1998–2005 for TRMM 3B42, and 1998–2005 for MI. For precipitation amount, frequency and intensity comparison, which are more sensitive to data periods, we used a common period of 2003–2005. For global and large-scale analyses in this study, the 0.25° gridded data were simply averaged to a 2° grid on which the surface data were derived (MI data were kept on their original 2.5° grid), so that the various data sets are more comparable in terms of spatial averaging. This is especially important for frequency and intensity comparisons (for which the MI is not included) because these two variables are very sensitive to spatial and temporal averaging. The multi-year averaged, composite hourly or 3-hourly data at each grid box for each season were then used to estimate the amplitude and phase of the diurnal (24 h, S_1) and semi-diurnal (12 h, S_2) harmonics using least squares fitting. To help gauge the significance of the diurnal variations, the amplitude is normalized (i.e., divided) by the daily mean and expressed in a percentage. We realize that the harmonic analysis is just one (albeit widely used) of many ways (e.g., Dai et al. 1999) to quantify the diurnal variations and it might not be the best approach for cases where the diurnal cycle is severely non-harmonic (Yang and Smith 2006).

Besides analyzing precipitation amount, precipitation frequency and intensity were also computed and analyzed. The frequency is defined here as the percentage of the observations (out of all valid observations) having a pre-defined precipitation event, while the intensity is the mean precipitation rate averaged over the precipitation events only (i.e., non-precipitating periods are excluded in this averaging). We used both daily (defined as >1 mm/day) and hourly or 3-hourly (>0.1 mm/h) precipitation in computing daily precipitation frequency and intensity (for seasonal map comparisons) and hourly or 3-hourly precipitation frequency and intensity (for diurnal analyses), respectively.

3 Mean precipitation amount, frequency, and intensity

Before analyzing the diurnal cycle, we first compare the spatial distribution of multi-year (2003–2005) mean precipitation amount, frequency, and intensity among the

Table 1 Precipitation data sets used in this study

Dataset name (Reference)	Spatial and temporal resolution and coverage	Data sources and merging method	Online documentation
CMORPH (Joyce et al. 2004)	0.25° grid, 60°S–60°N, 180°W–180°E; 30 min., 12/2002–present	Microwave estimates from the DMSP 13, 14 and 15 (SSM/I), the NOAA-15, 16 and 17 (AMSU-B) and the TRMM (TMI) satellites are propagated by motion vectors derived from geostationary satellite infrared data.	http://www.cpc.ncep.noaa.gov/products/janowiak/cmorph_description.html
PERSIANN (Hsu et al. 1997)	0.25° grid, 60°S–60°N, 180°W–180°E; 30 min., 3/2000–present	A neural network, trained by precipitation from TRMM TMI (2A12) and other satellites (DMSP F13, F14 and F15 (SSM/I), NOAA-15, 16, 17), was used to estimate 30 min. precipitation from infrared images from global geosynchronous satellites	http://hydis8.eng.uci.edu/persiann/
TRMM 3B42 (Huffman et al. 2007)	0.25° grid, 50°S–50°N, 180°W–180°E; 3- hourly, 1/1998–present	Microwave (TRMM, SSM/I, AMSR and AMSU) precipitation estimates were used to adjust IR estimates from geostationary IR observations. The rainfall estimates were scaled to match the monthly rain-gauge analysis used in TRMM 3B-43	http://daac.gsfc.nasa.gov/precipitation/TRMM_README/TRMM_3B42_readme.shtml
Merged microwave only precipitation (MI; X. Lin, personal communication)	2.5° grid, up to 75°S– 75°N, 180°W–180°E; hourly, 12/1997–present	Estimates from TRMM TMI, SSM/I on DMSP F13, F14, F15, and AMSR-E from AQUA were first averaged on a 0.25° grid and then further averaged to a 2.5° grid.	
CPC Hourly US Precipitation (Higgins et al. 1996)	2.5° lon × 2.0° lat, 20°N– 60°N, 140°W–60°W; hourly, 7/1948–10/2002	Hourly reports from ~2,800 rain-gauges were used to derive the gridded data	http://www.cpc.ncep.noaa.gov/research_papers/ncep_cpc_atlas/1/toc.html
Global precipitation frequency data (Dai 2001a,b)	2° grid, global; 3-hourly for each season, 1976– present	Weather reports from ships and over 15,000 stations were used to compile the occurrence frequency for various types of precipitation.	http://www.cgd.ucar.edu/cas/adai/
GPCP v2 (Adler et al. 2003)	2.5° grid, globe, monthly, 1979–present	IR estimates were calibrated by microwave estimates and then adjusted by rain-gauge data	http://precip.gsfc.nasa.gov/
CMAP (Xie and Arkin 1997)	2.5° grid, globe, monthly, 1979–present	Rain-gauge data over land, satellite IR, OLR, MSU and SSM/I estimates over ocean and model data (mostly over polar regions) were merged together, with oceanic rainfall calibrated by rain-gauge data from coastal and atoll stations	ftp://ftp.cpc.ncep.noaa.gov/precip

CMORPH Climate Prediction Center (CPC) morphing method, *PERSIANN* Precipitation Estimation from Remotely Sensed Information using Artificial Neural Networks, *TRMM* Tropical Rainfall Measuring Mission, *GPCP* Global Precipitation Climatology Project, *CMAP* Climate Prediction Center (CPC) Merged Analysis of Precipitation, *DMSP* the Defense Meteorological Satellites Program, *SSM/I* the Special Sensor Microwave Imager, *AMSU* the Advanced Microwave Sounding Unit, *TMI* the TRMM Microwave Imager, *AMSR* the Advanced Microwave Scanning Radiometer, *OLR* outgoing longwave radiation, *MSU* Microwave Sounding Unit

satellite data sets. Figure 1 shows June–August (JJA) mean precipitation amount from GPCP v2 and the differences between five other satellite products and the GPCP data. The GPCP precipitation shows large-scale patterns that are common in all the satellite products, but difference maps reveal substantial discrepancies among these datasets. The difference between the CMAP and GPCP illustrates current uncertainties in estimating global precipitation fields. The CMAP precipitation is generally higher than GPCP over low-latitude oceans due to its calibration using coastal and atoll gauge data, whose use to calibrate open-ocean precipitation has been questioned (Yin et al. 2004). Over land, the CMAP is generally lower than GPCP, which partly results from differences in the analysis techniques and the

climatological adjustment for wind-induced under-catch errors used by GPCP (although this error is most pronounced in cold seasons at high latitudes). The difference between TRMM 3B42 and GPCP is relatively small over most areas, which reflects the fact that the two products are heavily influenced by the same rain-gauge data from the Global Precipitation Climatology Centre (GPCC) and that GPCP used a linear combination of all satellite estimates. On the other hand, the other three products [CMORPH (similar for CMORPHmi), PERSIANN, MI] all show wet biases over many land areas and dry biases over many oceans. In particular, all these three products have large (>40%) wet biases over the United States, Central America, and tropical Africa. Large dry biases exist over the

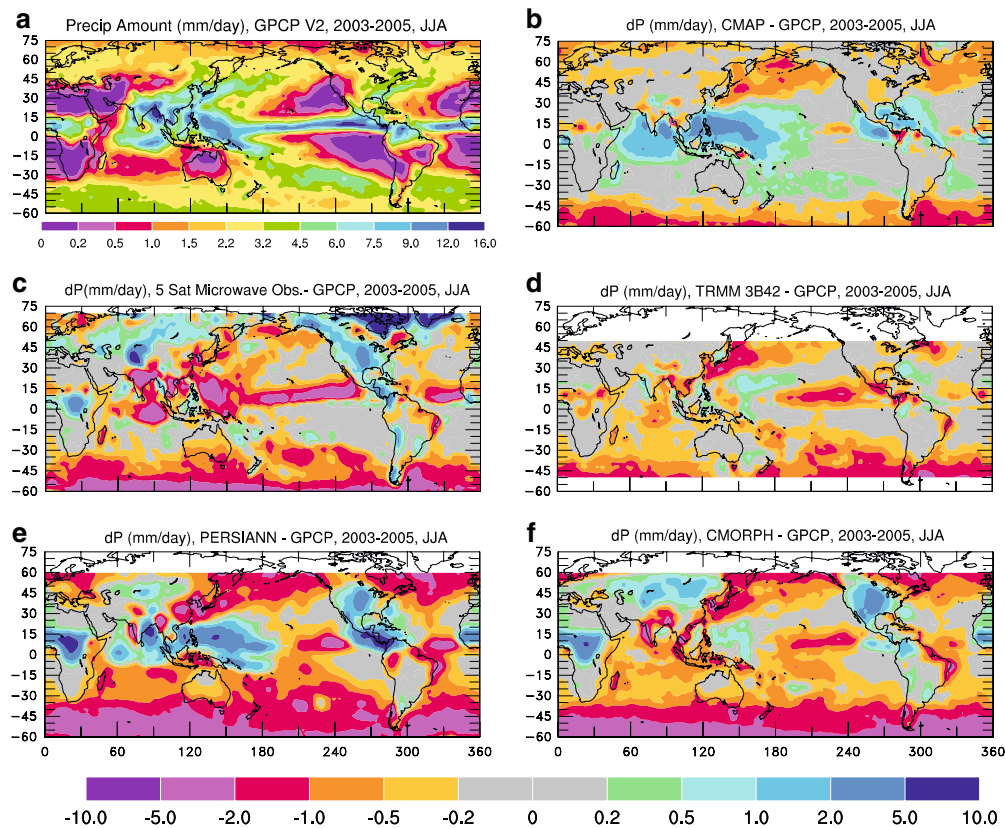


Fig. 1 2003–2005 mean June–August precipitation from GPCP (Adler et al. 2003), and the difference between CMAP (Xie and Arkin 1997) and GPCP (top right) and between each of the four pure satellite estimates and GPCP

Southern Ocean, which arises partly because current microwave estimates from polar-orbiting satellites are unreliable for high latitudes (above 50°). Plots of December–February (not shown) revealed similar difference patterns, except that the wet biases for CMORPH, PERSIANN, and MI are seen over almost all Southern Hemisphere land, and the biases become negative over the eastern U.S. Thus, compared with GPCP v2, the microwave calibrated precipitation from CMORPH, PERSIANN, and MI tends to overestimate warm-season land precipitation and underestimate oceanic precipitation, except for the western Pacific where PERSIANN and, to a lesser extent, CMORPH overestimate rainfall.

Figure 2 shows the 2003–2005 mean DJF and JJA frequency of daily precipitation (>1 mm/day) from CMORPHmi and merged products, PERSIANN, and TRMM 3B42. They are compared with estimates based on synoptic weather reports (Fig. 2a, f). The broad patterns of the frequency maps are comparable among the satellite products and they are similar to those of mean precipitation amount (cf. Fig. 1a), although PERSIANN shows higher DJF frequency in northern mid-latitudes than the other products. All the satellite products show less than 1% of the days with precipitation exceeding 1 mm/day over the

subtropical oceans and Africa. The inter-tropical convergence zone (ITCZ) is clearly shown in the frequency maps with a maximum frequency of 60–80%, although it is weak in PERSIANN over the central and eastern Pacific Ocean for DJF. The highest frequency ($>80\%$) is seen over tropical Africa and South America. There are large seasonal variations in the frequency over the mid-latitudes over both land and oceans and in the Tropics associated with the north–southward migration of the ITCZ. The microwave-only product from CMORPH (Fig. 2b, g) shows frequency maps very similar to the other products that also use IR data. This suggests that the inclusion of the IR observations, which improves sampling, does not alter the daily precipitation frequency significantly. The 3-hourly weather reports (Fig. 2a, f) show frequencies comparable to the satellite-based frequencies over most land areas, but the estimates over the oceans are based on limited 6-h sampling and thus have large sampling errors (Dai 2001a).

Daily precipitation intensity for DJF and JJA from the four different satellite products is shown in Fig. 3. Again, the broad patterns are similar among these products, with stronger intensity over the tropical oceans (10–16 mm/day) than most other regions (1.6–8.0 mm/day). The intensity patterns resemble less of those in precipitation amount (cf.

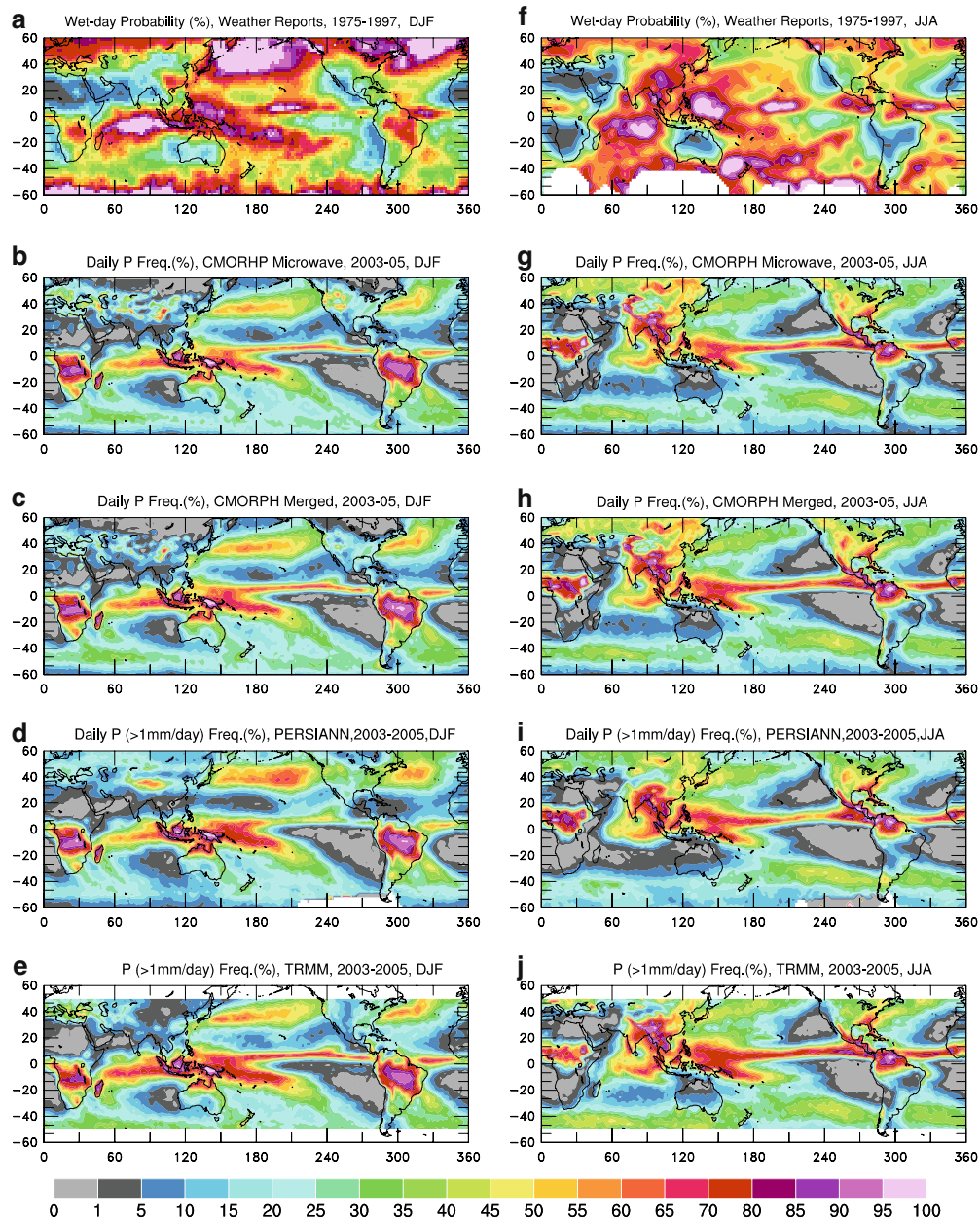


Fig. 2 2003–2005 mean DJF (left column) and JJA (right column) daily precipitation (>1 mm/day) frequency (%) from microwave only (2nd row, from CMORPH), merged CMORPH (3rd row), PERSI-

ANN (4th row), and TRMM 3B42 (bottom row) satellite products. Also shown (top row) are estimates based on synoptic weather reports (1975–1997 mean, Dai 2001b)

Fig. 1a) than the frequency (cf. Fig. 2), suggesting that spatial distribution of precipitation amount is firstly determined by how frequent it rains at different locations and secondarily by how heavy it rains. Figure 3 (top two rows) also shows that the inclusion of IR data does not change the intensity significantly. Quantitative differences do exist, however, among the different products. For example, the PERSIANN data show stronger intensity over the tropical western Pacific and Indian Ocean than TRMM 3B42.

In summary, the high-resolution, pure satellite products of hourly or 3-hourly precipitation show spatial patterns in mean precipitation amount that are comparable to GPCP monthly data, with some wet biases over warm-season land areas in CMORPH, PERSIANN, and MI. The daily precipitation frequency and intensity maps are comparable among these different data sets, and consistent with estimates based on weather reports over land. The use of IR data to improve sampling in the satellite products does not

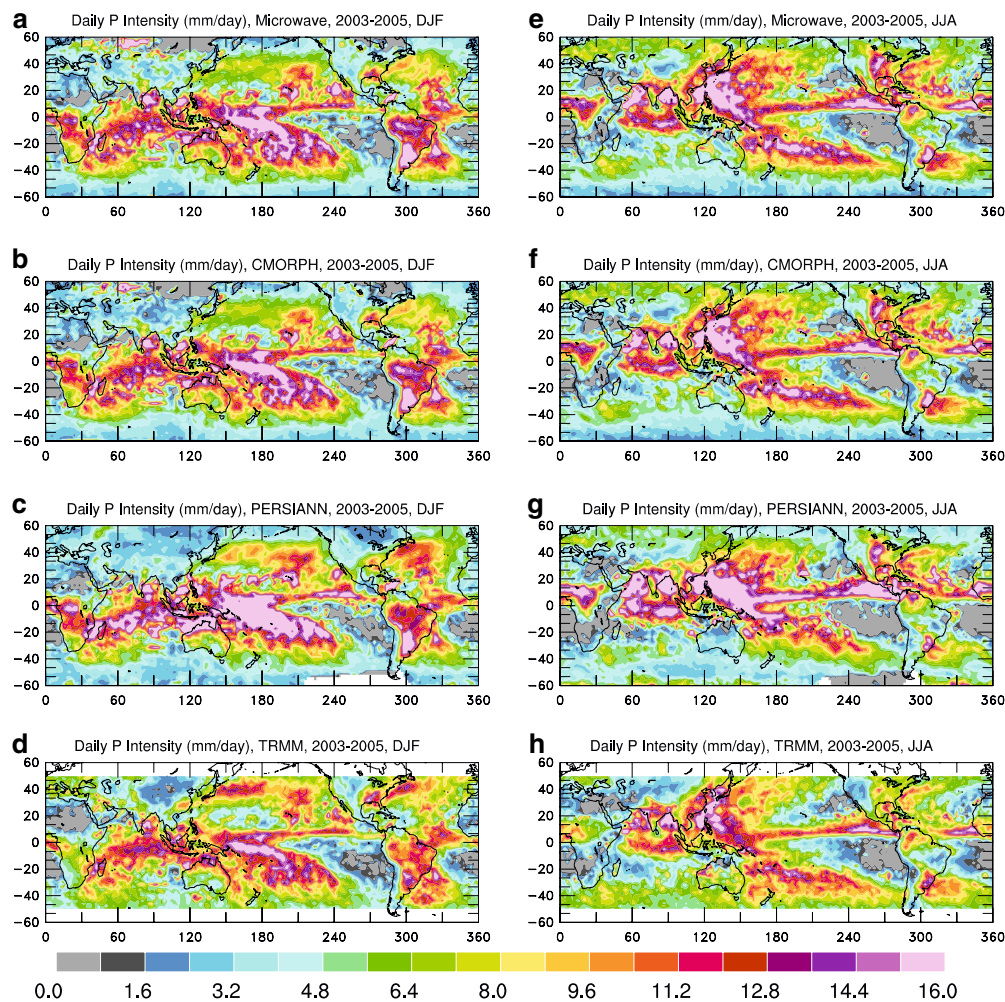


Fig. 3 Same as Fig. 2 but for daily precipitation intensity (mm/day) from satellite observations

change the mean precipitation amount, frequency, and intensity significantly.

4 The mean diurnal (24 h) harmonic of precipitation amount

Figure 4 shows the multi-year mean diurnal cycle of summer precipitation from ten selected 2° boxes around the world (see Fig. 5a for the locations on a map) derived from the four satellite products, surface weather reports (+), and rain-gauge measurements (thick solid line, for Fig. 4a only). In general, these data show comparable diurnal variations at these sites, with the weather reports being slightly noisier. For example, all the data show a large peak around 1700 LST at the S.E. U.S. box (with the rain-gauge data showing a smaller peak and a slightly earlier phase) (Fig. 4a), and a strong peak around 0700–0800 LST for DJF precipitation at the S. American box

(57°W , 29°S) (Fig. 4i, also cf. Fig. 6). Substantial diurnal variations are also evident for several other sites (e.g., Europe, E. China, and S.E. Australia), although the diurnal cycle is relatively weak at the oceanic sites such as the North Pacific and North Atlantic boxes (Fig. 4d, e), where the estimated diurnal phase can differ substantially among the different data sets. This is a common problem in estimating the diurnal phase for places with weak diurnal variations. Figure 4 also shows that the 24-h cycle predominates over 12 h and shorter time scale variations, with only the Sahel site showing a weak secondary peak around 1900 LST. However, the absence of a secondary peak does not necessarily imply non-existence of a semi-diurnal cycle.

The phase and amplitude of the diurnal (24 h) harmonic (S_1) estimated from surface weather reports and the four satellite products are shown in Fig. 5 for JJA precipitation (CMORHPmi is similar to CMORPH merged shown in the figure). We recognize that in Fig. 5 the

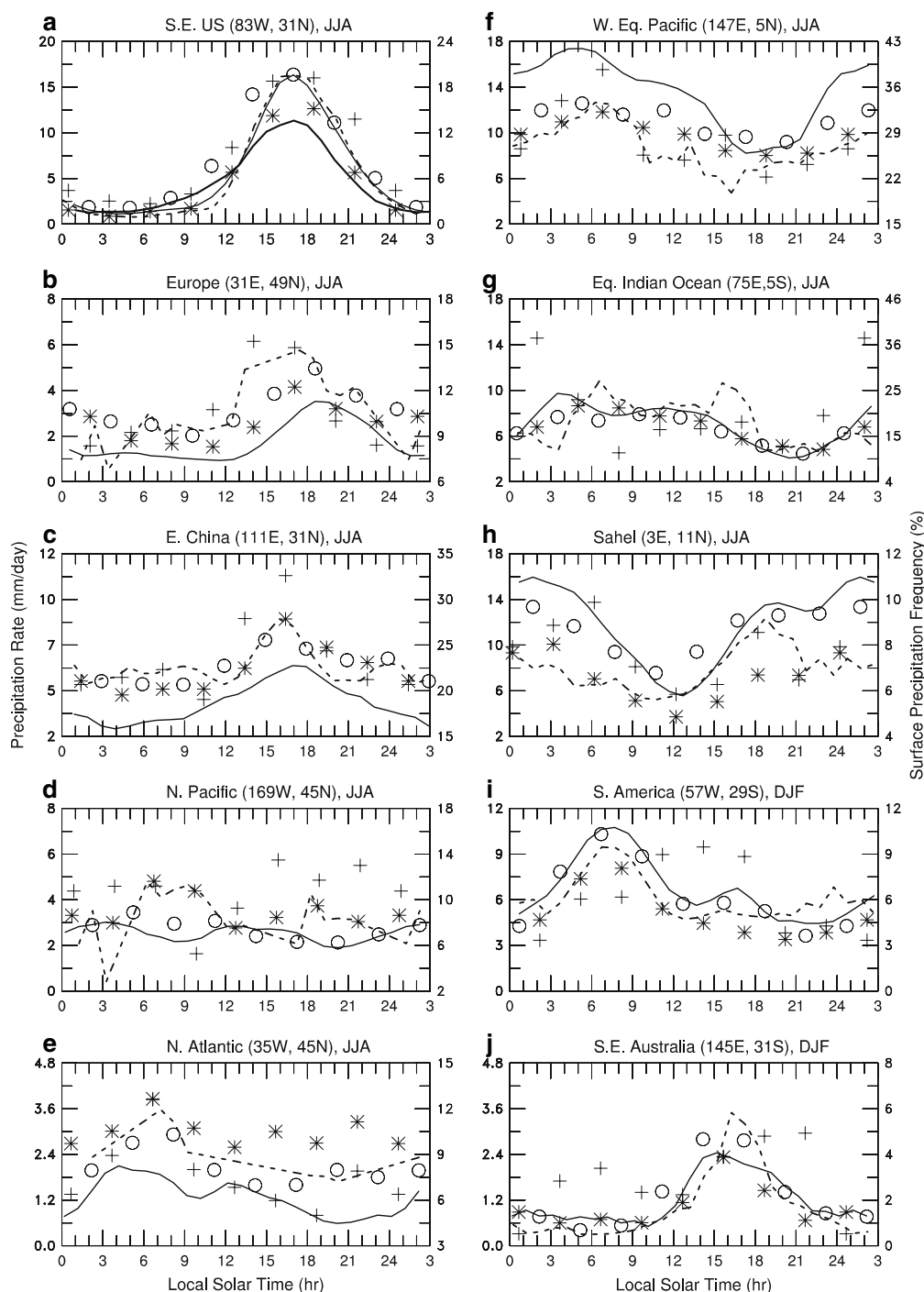


Fig. 4 Mean diurnal cycle of summer precipitation at ten selected $2^\circ \times 2^\circ$ boxes from surface weather reports (*plus* indicates frequency in % on the *right-hand ordinate*, 1975–1997 mean), CMORPH (*open circle* indicates 2003–2005), TRMM 3B42 (*asterisks* indicates 1998–2005), PERSIANN (*thin solid lines* indicates 2002–2005), and MI

(*dashed lines* indicates 1998–2005). Also shown in the *top-left panel* (*thick solid line*) is rain-gauge hourly data (for 1963–1993). Note that the hourly data were smoothed using a three-point running mean. See Fig. 5a for the location of the boxes (*black dots*) on a world map

weather reports, which are the only global surface data available, represent the diurnal cycle of precipitation frequency, whose diurnal phase and amplitude may differ from those of precipitation amount (see below) although

this is not the case in the rain-gauge data over the U.S. (Dai et al. 1999). Overall, both the surface and satellite data show an afternoon–evening maximum over most continental areas, while the peak is from midnight to

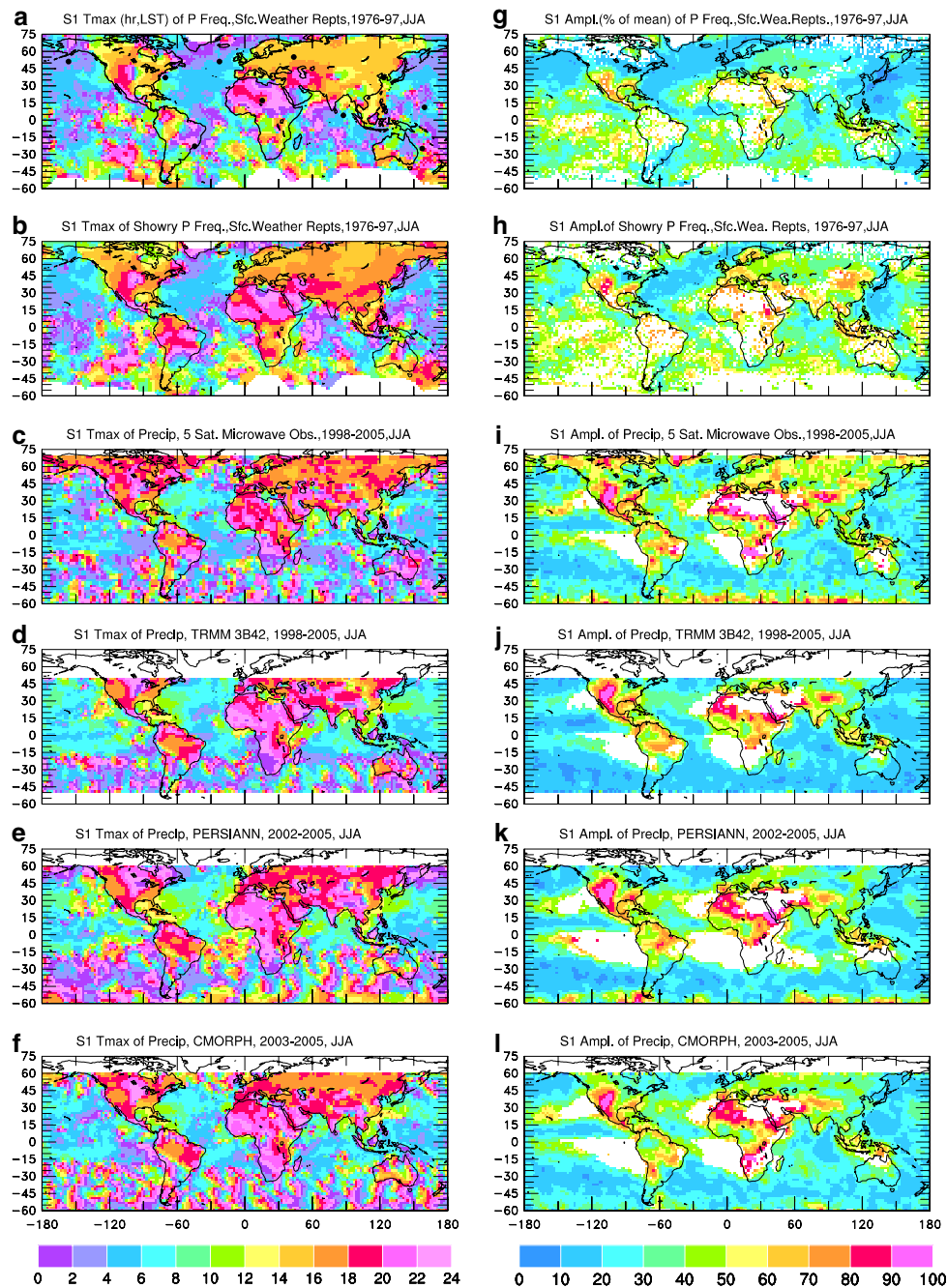


Fig. 5 The phase (local solar time in hours of the maximum, *left column*) and amplitude (in % of daily mean, *right column*) of the 24-h harmonic estimated from the mean diurnal anomalies of JJA precipitation frequency for non-drizzle and showery precipitation from surface weather reports (*top two rows*), and of JJA precipitation

amount from MI (*3rd row*), TRMM 3B42 (*4th row*), PERSIANN (*5th row*), and CMORPH (*bottom row*). Note the normalized amplitude is not shown (i.e., *white color*) over the subtropical areas where the mean precipitation is less than 0.1 mm/day. The *ten black dots* in *Fig. 4*

early morning over the oceans. The amplitude ranges from ~30 to 100% of the daily mean precipitation over most land areas and some oceans. A relative amplitude of 30% would mean a minimum-to-maximum difference equaling 60% of the daily mean, which is a substantial variation (cf. Fig. 4). The surface data (for both showery

and non-drizzle precipitation) are noisy over the tropical and southern oceans due to large sampling errors, but they do show spatially coherent phase patterns over the continents and many oceanic regions. For example, the surface weather reports (of JJA non-drizzle precipitation) (Fig. 5a) show the phase transition from the Rocky

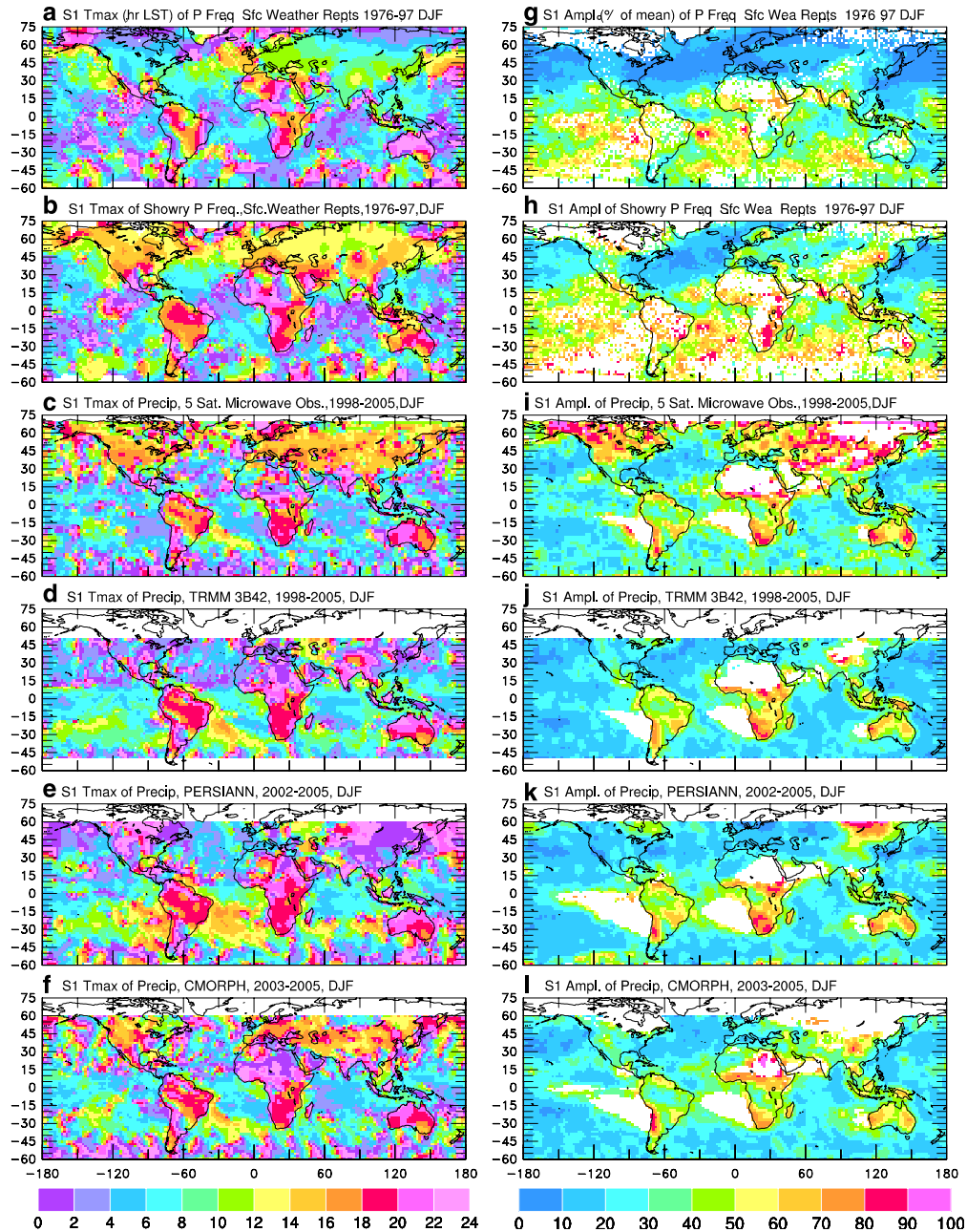


Fig. 6 Same as Fig. 5 but for December–February

Mountains to the central United States as seen in hourly rain-gauge data (e.g., Dai et al. 1999). They also show a phase shift from the central (~0400–0600 LST) to coastal (~0600–0800 LST) North Atlantic. This 2 h phase shift is also evident in the North Pacific. All the surface and satellite data show a morning maximum with an amplitude of 20–40% over a region around Uruguay and northeastern Argentina, although the surface observations extend the morning maximum farther to the west (Fig. 5). The estimated phase is noisy over the Southern Oceans,

where the uncertainties are large due to small amplitudes and large sampling errors.

The phase from the satellite data is about a few hours later than the surface observation over most land and oceans (Fig. 5). It is closer to the phase of showery precipitation frequency than all-form precipitation in weather reports, especially for the CMORPH (CMORPHmi is similar) and MI products. In contrast to this general bias, however, the early morning maximum over the central U.S. in the surface observation becomes a midnight peak in the

satellite precipitation. The MI and CMORPH seem to match the phase in surface data better than the PERSIANN and TRMM, which have a phase delayed further by ~1–2 h. The relative amplitudes over many land areas are larger in the satellite data than the surface observations, but they are comparable among the four satellite products (except for the subtropical oceans and arid land areas where the relative amplitudes are exaggerated by the small daily mean).

It is unclear what have caused these quantitative differences. While the surface weather reports have sampling

errors, especially over the tropical and southern oceans, they agree with rain-gauge data over the U.S. (Dai et al. 1999) and the sampling over the North Atlantic and Pacific Ocean appears to be sufficient (Dai 2001a, b). The fact that the diurnal phase from the satellite data matches that of the showery precipitation better than non-drizzle precipitation suggests that the satellite estimates of surface precipitation were biased toward convective events. This is probably not surprising given that IR sensors measure brightness temperatures of cold cloud tops that are often associated with deep convection, and that

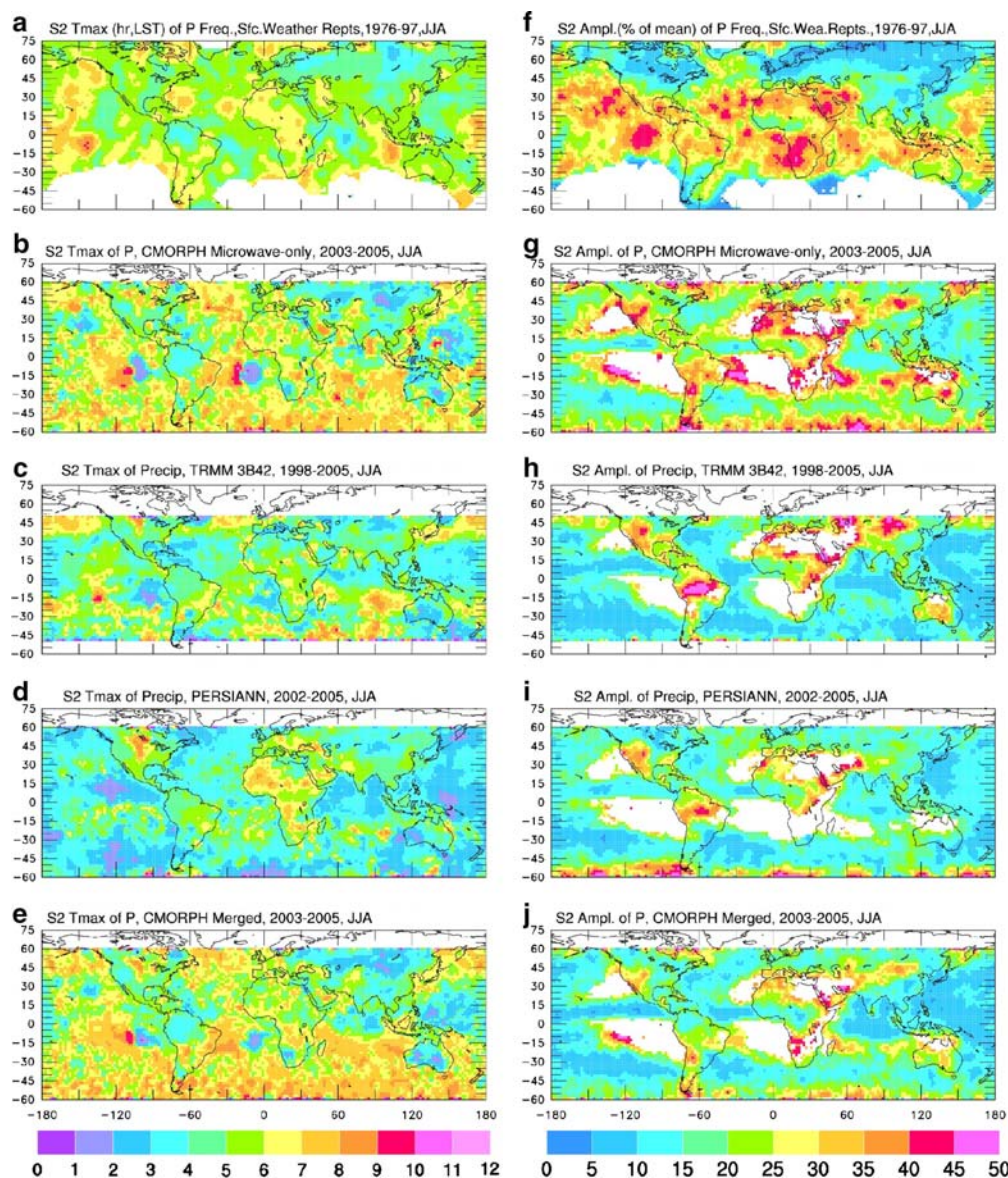


Fig. 7 The phase (local solar time in hours of the first maximum, *left column*) and amplitude (in % of daily mean, *right column*) of the 12-h harmonic estimated from the mean diurnal anomalies of JJA precipitation frequency for non-drizzle precipitation from surface weather reports (*top row*), and of JJA precipitation amount from

CMORPH microwave-only product (*2nd row*), TRMM 3B42 (*3rd row*), PERSIANN (*4th row*), and CMORPH merged product (*bottom row*). Note the normalized amplitude is not shown (i.e., *white color*) over the subtropical areas where the mean precipitation is less than 0.1 mm/day

microwave sensors are sensitive to the large hydrometeors in deep convective systems.

Figure 6 shows the diurnal phase and amplitude for boreal winter (December–February or DJF) precipitation. Over the northern mid-to-high latitudes, DJF precipitation

frequency has relatively small diurnal variations with amplitudes less than 30% of the daily mean and a peak in the morning (0600–1200 LST) (Fig. 6a, g). Winter showery precipitation over the northern latitudes peaks in the early afternoon (Fig. 6b). Over the oceans, the DJF

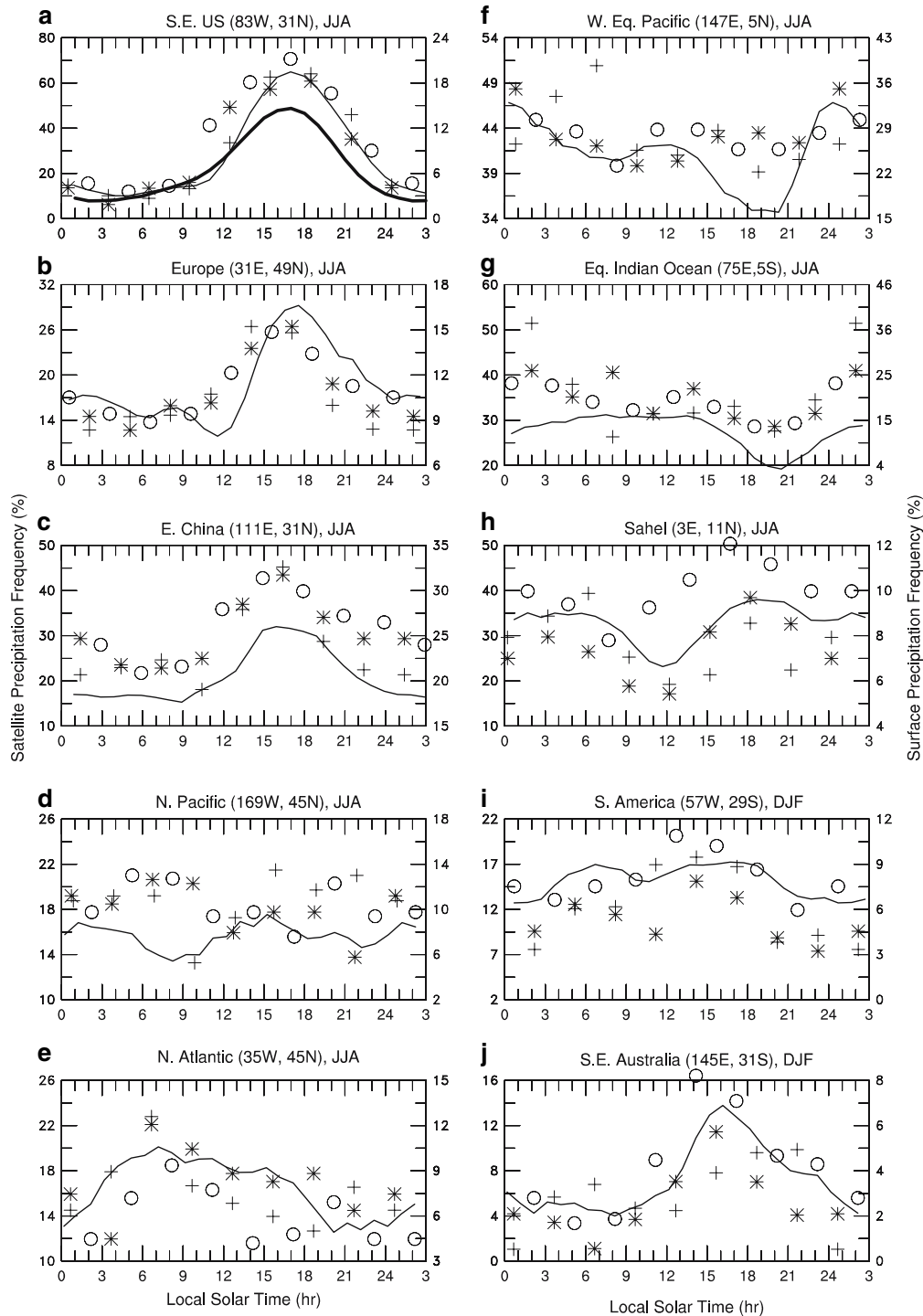


Fig. 8 Same as Fig. 4 but for the mean diurnal cycle of precipitation frequency

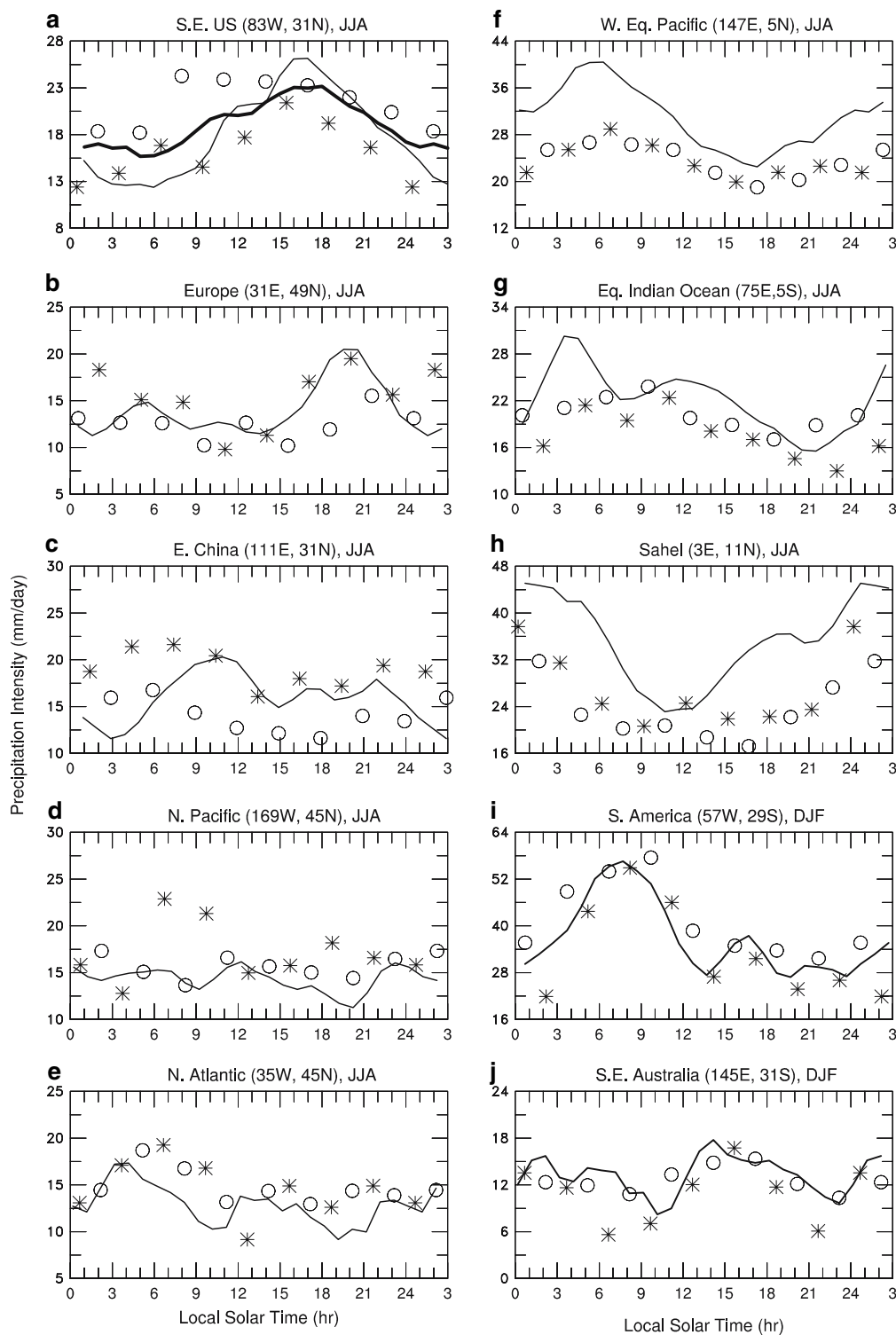


Fig. 9 Same as Fig. 4 but for the mean diurnal cycle of precipitation intensity

phase and amplitude are not very different to JJA (except that the DJF phase is about 1–2 h later), suggesting small seasonal variations in the diurnal cycle of oceanic precipitation.

The phase in the MI and CMORPH DJF precipitation is close to that of showery precipitation frequency from the weather reports, whereas the phase in PERSIANN and TRMM 3B42 is around midnight (~6 h earlier than

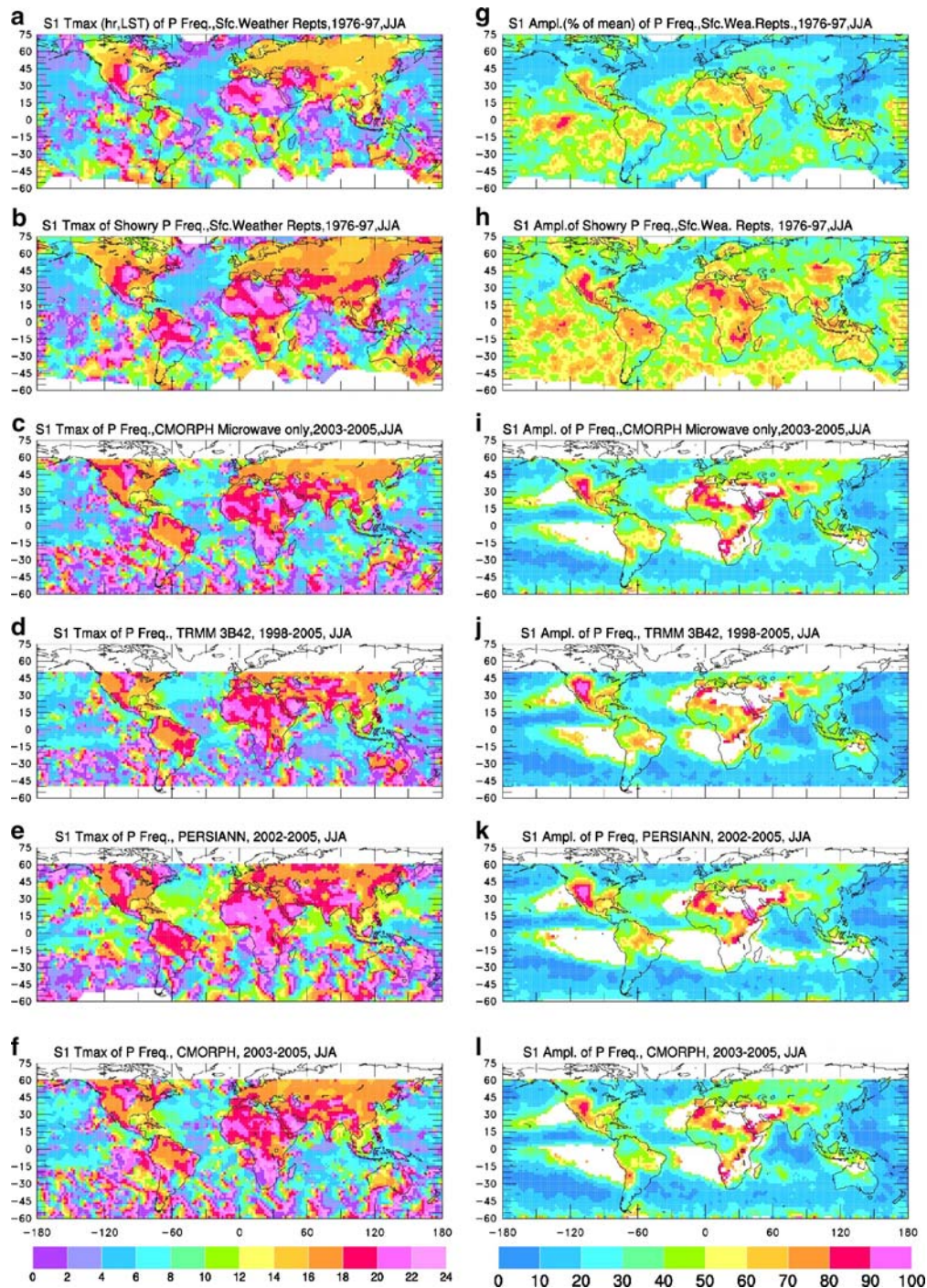


Fig. 10 Same as Fig. 5 but for precipitation *frequency* from weather reports and the satellite observations (in contrast to precipitation *amount* from satellite observations in Fig. 5)

non-drizzle precipitation frequency) for the northern latitudes (Fig. 6). The diurnal amplitude for MI (Fig. 6i) is too large over most Asia and N. America compared with the other products. Over the Southern Hemisphere, the satellite DJF data capture the late afternoon–evening

(1600–2000 LST) maximum in showery precipitation over continents and the late morning maximum over most oceans. The DJF results further suggest that the satellite data, especially MI and CMORPH, mainly capture the diurnal phase of convective precipitation.

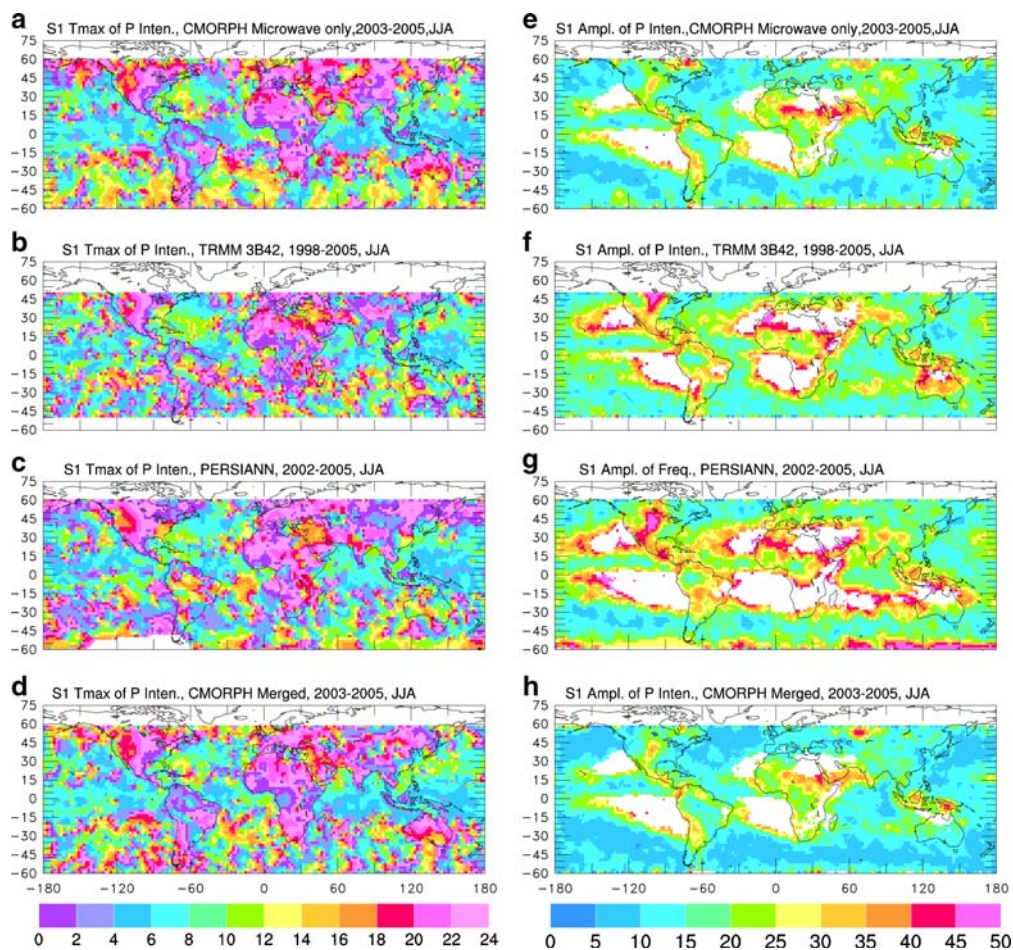


Fig. 11 Same as Fig. 5 but for precipitation intensity from satellite observations

5 The mean semi-diurnal (12 h) harmonic of precipitation amount

The 12-h, semi-diurnal cycle is generally weak and is resolved relatively poorly by 3-hourly data compared with the diurnal cycle. As such, the estimates presented here may contain large errors.

Figure 7 shows the mean phase and amplitude of the 12-h harmonic (S_2) estimated from the surface and satellite precipitation data for JJA. The relative amplitude is less than 20% over most land and oceans except for the dry areas with small mean precipitation in all satellite products. Surface weather reports also show small (5–15%) amplitudes over most of Eurasia and North America, but larger amplitudes over many low-latitude areas where sampling for the 12-h harmonic is less than adequate, especially over the oceans (Dai 2001a). The S_2 phase is similar for the TRMM and PERSIANN precipitation over most mid- and high-latitudes, with the time of maxima ranging from 0300 to 0600 LST, which is comparable to 0400–0600 LST in the surface weather reports and the phase in station records

(Hamilton 1981; Oki and Musiak 1994). The CMORPH precipitation (for both versions) shows a phase that is a few hours later than the other data sets over most oceans. The relative amplitude in the CMORPH microwave-only precipitation is slightly stronger than that in the other satellite products over arid regions.

6 The diurnal cycle of precipitation frequency and intensity

Precipitation diurnal variations arise mostly from its frequency rather than intensity in U.S. hourly rain-gauge data (Dai et al. 1999). To examine whether this is true over other parts of the world, we analyzed the diurnal cycle of precipitation frequency and intensity (see Sect. 2 for their definitions). Figures 8 and 9 show the multi-year mean diurnal cycle of precipitation frequency and intensity, respectively, at the ten selected grid boxes as in Fig. 4. For the sites with large diurnal cycles in precipitation amount, such as the S.E. U.S., Europe, S.E. Aus-

tralia, and Sahel boxes (cf. Fig. 4), the frequency and intensity both show considerable diurnal variations (Figs. 8, 9). Furthermore, the relative amplitude (i.e., divided by the daily mean) is larger in the frequency than intensity for the S.E. US, Europe, SE Australia, and some other sites, although the intensity is the dominant contributor for the S. America and Sahel sites. While the timing of the diurnal peak for the frequency and intensity is both similar to that of precipitation amount at the S.E. U.S. box (except for CMORPH), it often differs between the frequency and intensity (Figs. 8, 9). The diurnal peak of the intensity becomes less obvious for many sites such as E. China, the North Atlantic and Pacific boxes, especially for CMORPH precipitation.

Figure 10 shows the local time of maximum and amplitude of the diurnal (24 h) harmonic of the JJA precipitation frequency. Overall, both the phase and amplitude are very similar to those of precipitation amount (cf. Fig. 5), except that the relative amplitude over land are slightly weaker in the frequency for the satellite data (note the top two rows are the same in Figs. 5, 10). For the TRMM and PERSIANN precipitation, the local time of maximum over most Eurasia is a couple of hours earlier in the frequency than the amount, making it closer to that in surface observations (Fig. 10). This is not the case for CMORPH precipitation, whose amount and frequency show similar diurnal phases (cf. Figs. 5f, 10f). Furthermore, the phase for both the amount and frequency is similar over North America and most Southern Hemisphere land in all the satellite products. The phase and amplitude maps for DJF precipitation frequency (not shown) are comparable to those of DJF precipitation amount (cf. Fig. 6).

The diurnal cycle of precipitation intensity (Fig. 11) is much weaker than that for the amount and frequency, with only about half of the relative amplitude for frequency over most land and oceans. The CMORPH precipitation intensity (for both the merged and microwave-only products) has an even smaller diurnal cycle than the TRMM and PERSIANN products (Figs. 9, 11). The time of maximum for the intensity is two or more hours later than that in the frequency. It is around midnight (2200–0200 LST) over most land areas and in the late morning (0800–1000 LST) over many oceans. There are, however, many regional differences among the satellite products. For example, the CMORPH precipitation intensity (for both versions) has a peak in the morning over the Southeast U.S., in contrast to the afternoon peak in the PERSIANN and TRMM data (Fig. 11), although the later two are still about 2–4 h too early compared with rain-gauge data (Dai et al. 1999). Because of the relatively small amplitude, the estimated phase for intensity has large uncertainties (cf. Fig. 9).

7 Summary and concluding remarks

We have analyzed four high-resolution satellite precipitation products (namely, CMORPH, PERSIANN, TRMM 3B42, and MI) by comparing the spatial patterns in seasonal mean precipitation amount, daily precipitation frequency, and intensity, and the diurnal and semi-diurnal cycles among them and with surface observations, with a focus on the large-scale and global features. We found that these high-resolution data sets show spatial patterns in mean precipitation amount that are comparable to other monthly products (e.g., GPCP v2) at low- and mid-latitudes, with some wet biases over warm-season land areas and dry biases over some oceans in the CMORPH, PERSIANN, and MI precipitation compared with the GPCP precipitation. The difference between the TRMM and GPCP precipitation amount is small. The daily precipitation frequency and intensity maps are comparable among these pure satellite products, and consistent with the frequency estimated using synoptic weather reports over land. The spatial pattern in the frequency resembles that in the precipitation amount more than the intensity does, suggesting that precipitation spatial variations are largely determined by how often it rains rather than how heavy it rains at different locations. The use of IR data to improve sampling of individual events does not affect the mean precipitation amount, daily precipitation frequency and intensity significantly.

The satellite precipitation data show that sub-daily variations are dominated by the 24-h cycle, which has an afternoon–evening maximum and (mean-peak) amplitude of 30–100% of the daily mean in precipitation amount over most land areas during summer. Over most oceans, the 24-h harmonic has a peak from midnight to early morning with an amplitude of ~10–30% during both winter and summer. These diurnal results are broadly consistent with those based on surface weather reports. There are, however, quantitative discrepancies among the different satellite products and with the surface observations. In general, the time of maximum in the satellite precipitation is a few hours later than that in the surface observation over both land and ocean, and it is closer to the phase of showery precipitation frequency in weather reports, especially for the CMORPH and MI products. In the satellite products, the early-morning maximum over the central U.S. becomes a midnight peak, while the early-morning peak over most oceans is delayed to around 0800–1200 LST. The MI and CMORPH precipitation has a phase that is about 1–2 h earlier than that in the PERSIANN and TRMM data and thus matches the surface data better.

During boreal winter (DJF), surface weather reports show a weak diurnal cycle in precipitation frequency with an amplitude less than 30% and time of maximum around

0600–1200 LST over most Northern Hemisphere land and many oceanic areas, while the MI and CMORPH DJF precipitation shows a weak diurnal peak in the early afternoon over northern latitude land areas, which is close to that in showery precipitation in surface observations. The TRMM and PERSIANN DJF precipitation shows a weak maximum around midnight for the northern latitudes.

The satellite data and weather reports show a weak (amplitude <20%) semi-diurnal cycle over most land and oceans. The TRMM and PERSIANN precipitation exhibiting a coherent time of maximum around 0300–0600 LST over most mid- to high-latitudes, which is comparable to 0400–0600 LST in the surface data.

The satellite data confirm the previous notion (based largely on U.S. rain-gauge data) that the diurnal cycle of precipitation comes mostly from its frequency rather than its intensity over most of the globe. The phase and amplitude patterns of the diurnal cycle are similar for the precipitation amount and frequency, whereas the intensity has a much weaker amplitude (~half of that for frequency) and a phase several hours later than that for frequency.

These results suggest that the high-resolution precipitation products derived from multi-satellite observations are able to capture the mean spatial patterns in global precipitation fields, and produce comparable mean frequency and intensity maps for daily precipitation for the low- and mid-latitudes. They also capture much of the sub-daily variations in precipitation amount, frequency, and intensity, although quantitative differences in the diurnal phase and amplitude exist among the different products and with surface observations. In particular, the diurnal cycle in the satellite precipitation resembles that of showery or convective precipitation more than the total precipitation. Overall, the results suggest that these relatively new precipitation data sets can be used for many applications that require high temporal and spatial resolution, and that the inclusion of IR data from geostationary satellites appears to be an effective way to improve sampling without altering the frequency and intensity and the diurnal cycle significantly.

Acknowledgments The National Center for Atmospheric Research is sponsored by the National Science Foundation. This work was partly supported by NASA Grant No. NNX07AD77G and NCAR's Water Cycle Program.

References

- Adler RF, Huffman GJ, Chang A, Ferraro R, Xie P, Janowiak J, Rudolf B, Schneider U, Curtis S, Bolvin D, Gruber A, Susskind J, Arkin P, Nelkin E (2003) The version-2 Global Precipitation Climatology Project (GPCP) monthly precipitation analysis (1979–present). *J Hydrometeorol* 4:1147–1167
- Bowman KP, Collier JC, North GR, Wu QY, Ha EH, Hardin J (2005) Diurnal cycle of tropical precipitation in Tropical Rainfall Measuring Mission (TRMM) satellite and ocean buoy rain gauge data. *J Geophys Res* 110:D21104, doi:21110.21029/22005JD005763
- Carbone RE, Tuttle JD, Ahijevych DA, Trier SB (2002) Inferences of predictability associated with warm season precipitation episodes. *J Atmos Sci* 59:2033–2056
- Chang ATC, Chiu LS, Yang G (1995) Diurnal cycle of oceanic precipitation from SSM/I data. *Mon Weather Rev* 123:3371–3380
- Dai A (2001a) Global precipitation and thunderstorm frequencies. Part I: seasonal and interannual variations. *J Clim* 14:1092–1111
- Dai A (2001b) Global precipitation and thunderstorm frequencies. Part II: diurnal variations. *J Clim* 14:1112–1128
- Dai A (2006) Precipitation characteristics in eighteen coupled climate models. *J Clim* 19:4605–4630
- Dai A, Deser C (1999) Diurnal and semidiurnal variations in global surface wind and divergence fields. *J Geophys Res* 104:31109–31125
- Dai A, Fung IY, Del Genio AD (1997) Surface observed global land precipitation variations during 1900–88. *J Clim* 10:2943–2962
- Dai A, Giorgi F, Trenberth KE (1999) Observed and model-simulated diurnal cycles of precipitation over the contiguous United States. *J Geophys Res Atmos* 104:6377–6402
- Fujinami H, Nomura S, Yasunari T (2005) Characteristics of diurnal variations in convection and precipitation over the southern Tibetan Plateau during summer. *SOLA* 1:49–52
- Hamilton K (1981) A note on the observed diurnal and semi-diurnal rainfall variations. *J Geophys Res* 86:2122–2126
- Higgins WR, Janowiak JE, Yao Y-P (1996) A gridded hourly precipitation database for the United States (1963–1993). NCEP/Climate Prediction Center Atlas No. 1: US Department of Commerce, 47 pp
- Hong Y, Hsu KL, Sorooshian S, Gao XG (2005) Improved representation of diurnal variability of rainfall retrieved from the Tropical Rainfall Measuring Mission Microwave Imager adjusted Precipitation Estimation From Remotely Sensed Information Using Artificial Neural Networks (PERSIANN) system. *J Geophys Res* 110:D06102, doi:10.1029/2004JD005301
- Hsu KL, Gao XG, Sorooshian S, Gupta HV (1997) Precipitation estimation from remotely sensed information using artificial neural networks. *J Appl Meteorol* 36:1176–1190
- Huffman GJ, Adler RF, Morrissey MM, Bolvin DT, Curtis S, Joyce R, McGavock B, Susskind J (2001) Global precipitation at one-degree daily resolution from multisatellite observations. *J Hydrometeorol* 2:36–50
- Huffman GJ, Adler RF, Bolvin DT, Gu GJ, Nelkin EJ, Bowman KP, Hong Y, Stocker EF, Wolff DB (2007) The TRMM multisatellite precipitation analysis (TMPA): quasi-global, multiyear, combined-sensor precipitation estimates at fine scales. *J Hydrometeorol* 8:38–55
- Janowiak JE, Arkin PA, Morrissey M (1994) An examination of the diurnal cycle in oceanic tropical rainfall using satellite and in situ data. *Mon Weather Rev* 122:2296–2311
- Joyce RJ, Janowiak JE, Arkin PA, Xie PP (2004) CMORPH: a method that produces global precipitation estimates from passive microwave and infrared data at high spatial and temporal resolution. *J Hydrometeorol* 5:487–503
- Liang XZ, Li L, Dai A, Kunkel KE (2004) Regional climate model simulation of summer precipitation diurnal cycle over the United States. *Geophys Res Lett* 31:L24208, doi:24210.21029/22004GL021054
- Lin X, Randall DA, Fowler LD (2000) Diurnal variability of the hydrologic cycle and radiative fluxes: comparisons between observations and a GCM. *J Clim* 13:4159–4179

- Nesbitt SW, Zipser EJ (2003) The diurnal cycle of rainfall and convective intensity according to three years of TRMM measurements. *J Clim* 16:1456–1475
- New M, Todd M, Hulme M, Jones P (2001) Precipitation measurements and trends in the twentieth century. *Int J Climatol* 21:1899–1922
- Oki T, Musiak K (1994) Seasonal change of the diurnal cycle of precipitation over Japan and Malaysia. *J Appl Meteorol* 33:1445–1463
- Okumura K, Satomura T, Oki T, Khantiyanan W (2003) Diurnal variation of precipitation by moving mesoscale systems: radar observations in northern Thailand. *Geophys Res Lett* 30:2073, doi:10.1029/2003GL018302
- Pinker RT, Zhao Y, Akoshile C, Janowiak J, Arkin P (2006) Diurnal and seasonal variability of rainfall in the sub-Sahel as seen from observations, satellites and a numerical model. *Geophys Res Lett* 33:L07806, doi:10.1029/2005GL025192
- Sorooshian S, Hsu K-L, Gao X, Gupta HV, Imam B, Braithwaite D (2000) Evaluation of PERSIANN system satellite-based estimates of tropical rainfall. *Bull Am Meteorol Soc* 81:2035–2046
- Sorooshian S, Gao X, Maddox RA, Hong Y, Imam B (2002) Diurnal variability of tropical rainfall retrieved from combined GOES and TRMM satellite information. *J Clim* 15:983–1001
- Trier SB, Parsons DB (1993) Evolution of environmental-conditions preceding the development of a nocturnal mesoscale convective complex. *Mon Weather Rev* 121:1078–1098
- Wallace JM (1975) Diurnal variations in precipitation and thunderstorm frequency over conterminous United States. *Mon Weather Rev* 103:406–419
- Wang CC, Chen GTJ, Carbone RE (2004) A climatology of warm-season cloud patterns over east Asia based on GMS infrared brightness temperature observations. *Mon Weather Rev* 132:1606–1629
- Xie PP, Arkin PA (1997) Global precipitation: a 17-year monthly analysis based on gauge observations, satellite estimates, and numerical model outputs. *Bull Am Meteorol Soc* 78:2539–2558
- Xie PP, Chen MY, Joyce R, Janowiak JE, Arkin PA (2005) Diurnal cycle in the North America Monsoon. *Bull Am Meteorol Soc* 86:26–28
- Yang GY, Slingo J (2001) The diurnal cycle in the Tropics. *Mon Weather Rev* 129:784–801
- Yang S., Smith EA (2006) Mechanisms for diurnal variability of global tropical rainfall observed from TRMM. *J Climate* 19:5190–5226
- Yin XG, Gruber A, Arkin P (2004) Comparison of the GPCP and CMAP merged gauge-satellite monthly precipitation products for the period 1979–2001. *J Hydrometeorol* 5:1207–1222